

© 2019 by Akshat Puri. All rights reserved.

MEASUREMENT OF ANGULAR AND MOMENTUM DISTRIBUTIONS OF CHARGED  
PARTICLES WITHIN AND AROUND JETS IN Pb+Pb AND  $p\bar{p}$  COLLISIONS AT  
 $\sqrt{S_{NN}} = 5.02$  TeV WITH ATLAS AT THE LHC

BY  
AKSHAT PURI

DISSERTATION

Submitted in partial fulfillment of the requirements  
for the degree of Doctor of Philosophy in Physics  
in the Graduate College of the  
University of Illinois at Urbana-Champaign, 2019

Urbana, Illinois

Doctoral Committee:

Professor Matthias Grosse Perdekamp, Chair  
Professor Anne Marie Sickles, Advisor  
<sup>1</sup> Professor Aida El-Khadra  
Professor Bryce Gadaway

# Abstract

<sup>2</sup> Studies of the fragmentation of jets into charged particles in heavy-ion collisions can help in understanding  
<sup>3</sup> the mechanism of jet quenching by the hot and dense matter created in such collisions, the quark-gluon  
<sup>4</sup> plasma. This thesis presents a measurement of the angular distribution of charged particles around the jet  
<sup>5</sup> axis as measured in Pb+Pb and  $pp$  collisions collided at a center of mass energy of  $\sqrt{s_{NN}} = 5.02$  TeV. The  
<sup>6</sup> measurement is done using the ATLAS detector at the Large Hadron Collider, and utilizes  $0.49\text{ pb}^{-1}$  of  
<sup>7</sup> Pb+Pb and  $25\text{ pb}^{-1}$  of  $pp$  data collected in 2015. The measurement is performed for jets reconstructed  
<sup>8</sup> with the anti- $k_t$  algorithm with radius parameter  $R = 0.4$ , and is extended to regions outside the jet cone.  
<sup>9</sup> Results are presented as a function of Pb+Pb collision centrality, and both jet and charged-particle transverse  
<sup>10</sup> momenta. It was observed that in Pb+Pb collisions there is a broadening of the jet for charged particles with  
<sup>11</sup>  $p_T < 4$  GeV, along with a narrowing for charged particles with  $p_T > 4$  GeV. Ratios between the angular  
<sup>12</sup> distributions in Pb+Pb and  $pp$  showed an enhancement for particles with  $p_T < 4$  GeV in Pb+Pb collisions,  
<sup>13</sup> with the enhancement increasing up to 2 for  $r < 0.3$ , and remaining constant for  $0.3 < r < 0.6$ . Charged  
<sup>14</sup> particles with  $p_T > 4$  GeV show a small enhancement in the jet core for  $r < 0.05$ , with a growing suppression  
<sup>15</sup> of up to 0.5 for  $r < 0.3$  in Pb+Pb collisions. The depletion remains constant for  $0.3 < r < 0.6$ .

*For my Mother, Father, and Brother*

# **Contents**

<sup>18</sup>	<b>Chapter 1 Theoretical Introduction</b>	<b>1</b>
<sup>19</sup>	1.1 Quantum Chromodynamics	1
<sup>20</sup>	1.2 Heavy Ion Collisions and the Quark Gluon Plasma	4
<sup>21</sup>	1.2.1 Heavy Ion Collisions	4
<sup>22</sup>	1.2.2 The Quark Gluon Plasma	9
<sup>23</sup>	1.3 Jets and Jet Quenching	10
<sup>24</sup>		

# Chapter 1

## Theoretical Introduction

This section shall discuss the theoretical background necessary to understand jet measurements. It will discuss the fundamentals of quantum chromodynamics (QCD), the heavy ion collision system and the quark gluon plasma that is formed, and finally jets and jet energy loss.

### 1.1 Quantum Chromodynamics

Quantum Chromodynamics is a gauge theory with SU(3) symmetry that describes the dynamics of the strong interactions between quarks and gluons. It is part of the Standard Model [1], the building blocks of which are shown in Figure 1.1.

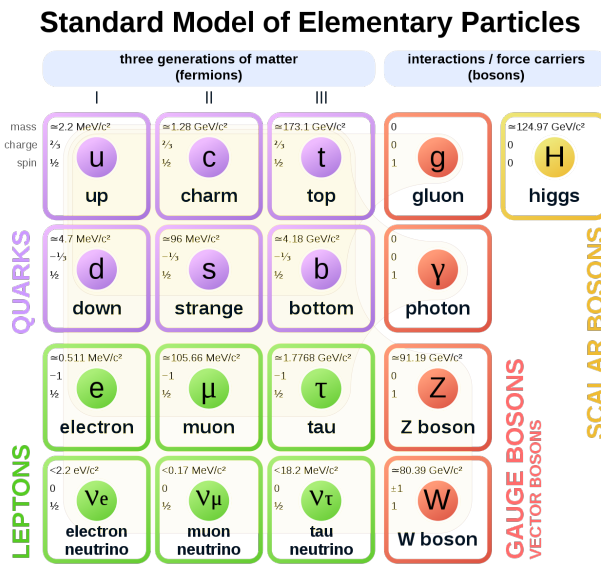


Figure 1.1: The elementary particles of the standard model.

Quarks are fermions with a spin of 1/2, and carry a fractional electric charge as well as a color charge. They all have mass and come in six flavors: up, down, top, bottom, strange, charm. The lightest quarks

<sup>34</sup> (u and d) combine and form stable particles, while the heavier quarks can only be produced in energetic  
<sup>35</sup> environments and decay rapidly. Gluons are gauge bosons (force carriers) with a spin of 1, and are what hold  
<sup>36</sup> quarks together. The dynamics of the quarks and gluons are described by the QCD Lagrangian given as [2]:

$$\mathcal{L}_{\text{QCD}} = \sum_q \bar{\psi}_{q,a} (i\gamma^\mu \partial_\mu \delta_{ab} - g_s \gamma^\mu t_{ab}^C \mathcal{A}_\mu^C - m_q \delta_{ab}) \psi_{q,b} - \frac{1}{4} F_{\mu\nu}^A F^{A\mu\nu} \quad (1.1)$$

<sup>37</sup> where  $\psi_{q,a}$  and  $\psi_{q,b}$  are quark-filled spinors for a quarks with flavor  $q$ , mass  $m_q$ , and color  $a$  and  $b$  respectively,  
<sup>38</sup> with the values for  $a$  and  $b$  ranging from 1 to 3 (for the three colors). The  $\mathcal{A}_\mu^C$  corresponds to the gluon field  
<sup>39</sup> with  $C$  taking values from 1 through 8 (for the 8 types of gluons). The  $t_{ab}^C$  corresponds to the Gell-Mann  
<sup>40</sup> matrices that are the generators of the SU(3) group, and dictate the rotation of the quarks color in SU(3)  
<sup>41</sup> space when it interacts with a gluon. The coupling constant is encoded within  $g_s$ , which is defined by  
<sup>42</sup>  $g_s \equiv \sqrt{4\pi\alpha_s}$ . The field tensor  $F_{\mu\nu}^A$  can be written in terms of the structure constants of the SU(3) group  
<sup>43</sup>  $f_{ABC}$ , and is given by:

$$F_{\mu\nu}^A = \partial_\mu \mathcal{A}_\nu^A - \partial_\nu \mathcal{A}_\mu^A - g_s f_{ABC} \mathcal{A}^B \mathcal{A}^C \quad (1.2)$$

<sup>44</sup> While many parallels can be drawn between Quantum Electrodynamics (QED, the theory that describes  
<sup>45</sup> photons and electrons) and QCD, the difference between the two comes from the gluon-gluon interactions  
<sup>46</sup> allowed in QCD, making it non-Abelian. These interactions can be summarized as shown in Figure 1.2.

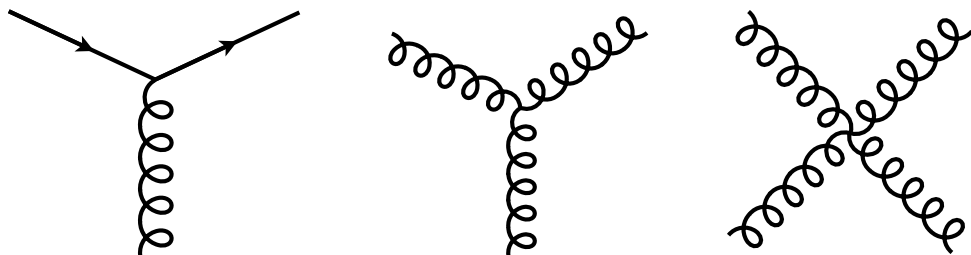


Figure 1.2: The allowed vertices in QCD. The vertices involving two or more gluons are unique to QCD and do not have a QED analog.

<sup>47</sup> A core feature of QCD is that the coupling constant  $\alpha_s$  has an energy dependence shown in Figure 1.3.  
<sup>48</sup> This dependence can be expressed in terms of the  $\beta$  function as

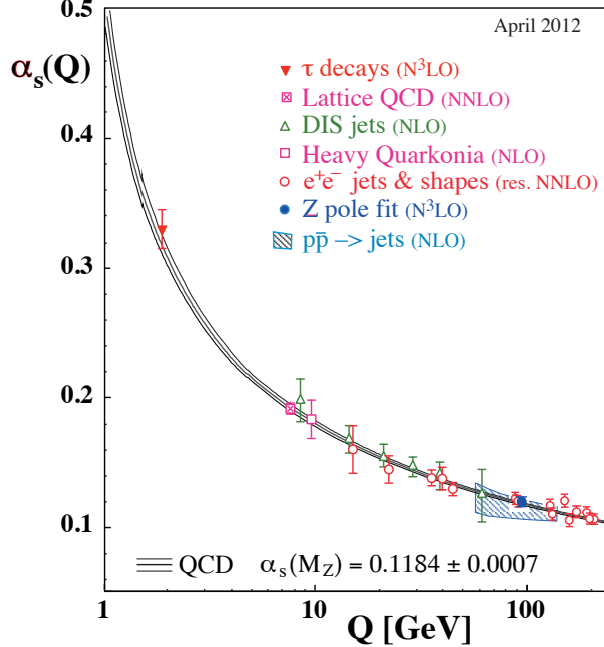


Figure 1.3: The running coupling constant  $\alpha_s$  as a function of the momentum transfer  $Q$ . Figure taken from Ref. [2].

$$Q^2 \frac{\partial \alpha_s(Q^2)}{\partial Q^2} = \beta(\alpha_s(Q^2)) \quad (1.3)$$

49 where  $Q$  is the momentum transfer in the particle reaction. The beta function can be expressed using  
50 perturbative QCD (pQCD) as

$$\beta(\alpha_s) = -(b_0 \alpha_s^2 + b_1 \alpha_s^3 + b_2 \alpha_s^4 \dots) \quad (1.4)$$

51 where the coefficients  $b_i$  depend on the number of colors and flavors.

52 This running coupling constant is small and asymptotically tends to zero at large energy scales (or at  
53 small distances) and is large at small energy scales (large distances). This running coupling phenomenon  
54 leads to two key behaviors: asymptotic freedom and color confinement.

55 **Asymptotic Freedom:** At high energy scales (small distances), the QCD coupling constant  $\alpha_s$  is  
56 small and tends to zero, implying a free particle behavior of quarks and gluons. This has been observed by a

57 variety of deep inelastic experiments [3–16]

58       **Color Confinement** The opposite end of the running coupling constant phenomenon is color confinement.  
59       This property of QCD forbids the direct observation of free quarks and gluons, allowing only for  
60       composite particles that are color singlets.

## 61       1.2 Heavy Ion Collisions and the Quark Gluon Plasma

62       Heavy ion collisions can be used as a tool to study the Quark Gluon Plasma [17] . They provide access to  
63       the otherwise confined partons, and give insight into the QCD phase diagram and the transition between the  
64       QGP and hadronic matter. This section will briefly discuss a heavy ion collision and the properties of the  
65       medium that is formed in such a collision.

### 66       1.2.1 Heavy Ion Collisions

67       In a heavy ion collision, the colliding nuclei are accelerated to relativistic energies and are Lorentz contracted  
68       discs. In the case of a Pb+Pb collision the relativistic  $\gamma$  factor is between 100 and 2500 for beam rapidities  
69       of  $y = 5.3$  and  $8.5$ . Each nucleus contains many colored quarks and antiquarks, with three more quarks than  
70       anti-quarks per nucleon, with the  $q\bar{q}$  popping in and out of the vacuum due to quantum fluctuations. These  
71        $q\bar{q}$  pairs are sources of transverse color fields and the corresponding force carriers, the gluons.

72       When these pancake like discs collide, their color fields interact and there is a color charge exchange,  
73       producing longitudinal color fields that fill the space between the receding discs. While the maximum energy  
74       density in the process occurs just at the collision, the energy density 1 fm/c after the collision is  $12 \text{ GeV/fm}^3$ ,  
75       much higher than the  $500 \text{ MeV/fm}^3$  in a typical hadron. Lattice QCD calculations in thermodynamics show  
76       that at these energies, the partons produced in the collision cannot be treated as a collection of distinct  
77       hadrons. In fact, these partons are strongly coupled to each other and form a medium called the Quark  
78       Gluon Plasma (QGP) [??].

79       After the collision the energy density between the receding nuclei starts to decrease as the QGP cools and  
80       expands. This process, seen in Figure 1.4, continues till the energy density drops to below that within a  
81       hadron and the fluid “hadronizes”. These individual hadrons briefly scatter off of each other before they  
82       freely fly towards the detector (freeze-out).

83       While Figure 1.4 shows snapshots of a head on (central) collision between two large nuclei, it is possible to  
84       have collisions where the impact parameter is larger and hence the overlap region is smaller. These collisions,

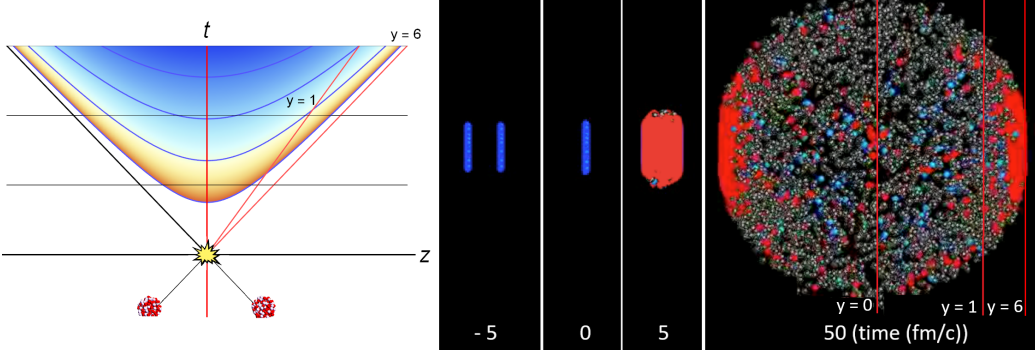


Figure 1.4: (left) Space-time diagram for a heavy ion collision. The color is indicative of the temperature of the QGP formed. (right) Snapshots of a heavy ion collision at  $\sqrt{s_{NN}} = 2.76$  TeV at different times. The Lorentz contracted nuclei are in blue while the QGP is in red. Figures from References [7, 8].

85 called peripheral collisions, qualitatively undergo the same process described above, with the size and shape  
86 of the QGP being different.

87 The basic parameters of a heavy ion collision such as the number of participants  $N_{\text{part}}$  and number of  
88 binary collisions  $N_{\text{coll}}$  can be determined using the Glauber Monte Carlo simulations [18, 19]. This technique  
89 considers a nucleus-nucleus collision as a collection of independent binary nucleon-nucleon collisions; the  
90 colliding nuclei are modeled as a set of uncorrelated nucleons being positioned within the nucleus based on a  
91 the nuclear density function uniform in azimuthal and in polar angles. The nuclear density function shown in  
92 Figure 1.5 for Au and Cu, is given by:

$$\rho(r) = \rho_0 \frac{1 + w(r/R)^2}{1 + e^{\frac{r-R}{a}}} \quad (1.5)$$

93 where  $\rho_0$  is the nucleon density,  $R$  is the nuclear radius,  $a$  is the skin depth,  $w$  corresponds to deviations  
94 from a circular shape and is typically zero for larger nuclei like Cu, W, Au, Pb, and U. For the Pb nuclei  
95 used at the LHC,  $w = 0$ ,  $R = 6.62$  fm and  $a = 0.55$  fm [20].

96 They are then arranged with a random impact parameter  $b$  based on the distribution  $d\sigma/db = 2\pi b$  and  
97 projected onto the  $x - y$  plane as shown in Figure 1.6. They are then made to travel on straight trajectories,  
98 colliding if  $d \leq \sqrt{\sigma_{\text{inel}}^{\text{NN}}/\pi}$ , where  $d$  is the distance between the nucleons in a plane transverse to the beam  
99 axis and  $\sigma_{\text{inel}}^{\text{NN}}$  is the inelastic scattering cross section. [21, 22]

100 An important parameter for colliding nuclei A and B with  $A$  and  $B$  nucleons is the thickness function  
101  $T_{AB}$ . It describes the effective overlap area in which specific nucleons in the two colliding nuclei can interact.  
102 It can be defined in terms of the probability per unit area of a given nucleon being located at a particular

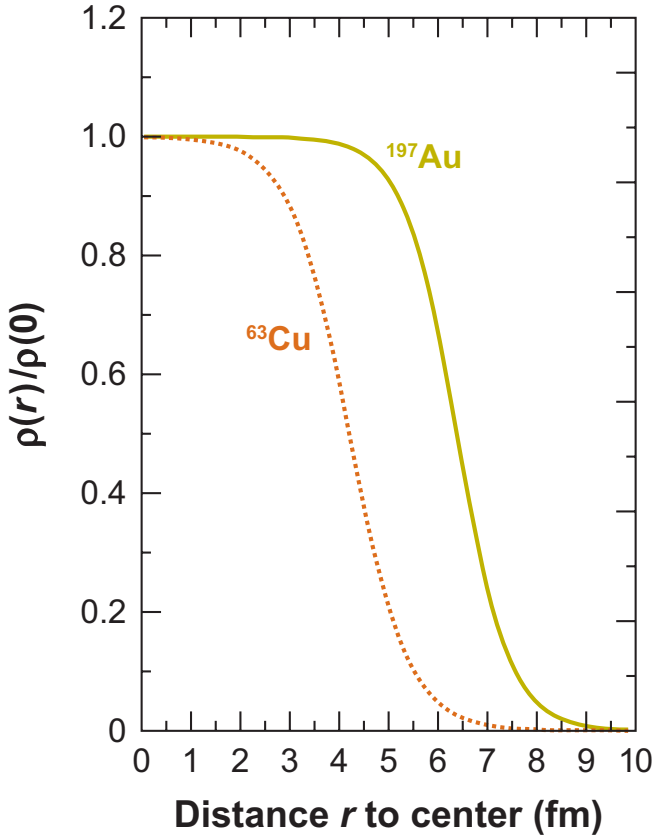


Figure 1.5: The nuclear density distributions for nuclei used at RHIC: Cu ( $w = 0$ ,  $R = 4.2$  fm and  $a = 0.48$  fm) and Au ( $w = 0$ ,  $R = 6.38$  fm and  $a = 0.535$  fm) [20, 21].

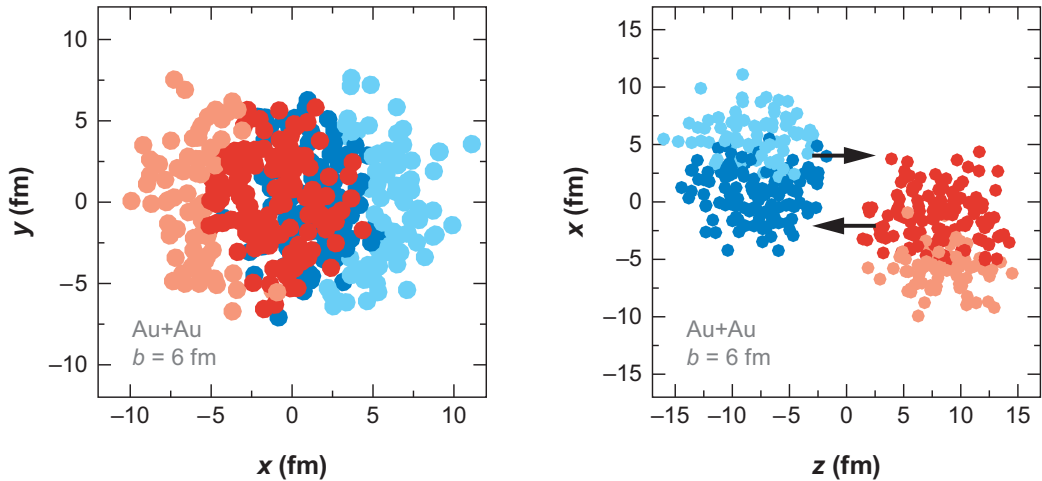


Figure 1.6: A Glauber Monte Carlo event for  $Au + Au$  at  $\sqrt{s_{NN}} = 200$  GeV with impact parameter of 6 fm viewed in the (left) transverse plane and (right) along the beam axis. Darker circles represent the participating nucleons. Taken from [21].

103 distance  $s$  within the nucleus. For the colliding nuclei  $A$  and  $B$ , this is given by  $T_A(\mathbf{s}) = \int \rho_A(\mathbf{s}, z_A) dz_A$  and  
 104  $T_B(\mathbf{s}) = \int \rho_B(\mathbf{s}, z_B) dz_B$ . Then,  $T_{AB}$  is given by

$$T_{AB}(\mathbf{b}) = \int T_A(\mathbf{s})T_B(\mathbf{s} - \mathbf{b}) d^2s \quad (1.6)$$

105 The probability of then having  $n$  interactions between nuclei  $A$  and  $B$  is given by the binomial distribution:

$$P(n, \mathbf{b}) = \binom{AB}{n} \left[ T_{AB}(\mathbf{b}) \sigma_{\text{inel}}^{\text{NN}} \right]^n \left[ 1 - T_{AB}(\mathbf{b}) \sigma_{\text{inel}}^{\text{NN}} \right]^{AB-n} \quad (1.7)$$

106 where the first term is the number of combinations for finding  $n$  collisions from  $AB$  possibilities, the  
 107 second term is the probability for having exactly  $n$  collisions, and the last term the probability of  $AB - n$   
 108 misses. Then the total probability of an interaction between A and B is

$$\frac{d^2 \sigma_{\text{inel}}^{\text{AB}}}{db^2} \equiv p_{\text{inel}}^{\text{AB}}(b) = \sum_{n=1}^{AB} P(n, \mathbf{b}) = 1 - \left[ 1 - T_{AB}(\mathbf{b}) \sigma_{\text{inel}}^{\text{NN}} \right]^{AB} \quad (1.8)$$

109 Then the total cross section is given by

$$\sigma_{\text{inel}}^{\text{AB}} = \int_0^\infty 2\pi b db \left[ 1 - \left( 1 - T_{AB}(\mathbf{b}) \sigma_{\text{inel}}^{\text{NN}} \right)^{AB} \right] \quad (1.9)$$

110 and  $N_{\text{coll}}$  and  $N_{\text{part}}$  are given by [23, 24]

$$N_{\text{coll}}(b) = \sum_{n=1}^{AB} n P(n, b) = AB \times T_{AB}(b) \sigma_{\text{inel}}^{\text{NN}} \quad (1.10)$$

$$N_{\text{part}}(b) = A \int T_A(\mathbf{s}) \left[ 1 - \left( 1 - T_B(\mathbf{s} - \mathbf{b}) \sigma_{\text{inel}}^{\text{NN}} \right)^B \right] d^2s + B \int T_B(\mathbf{s} - \mathbf{b}) \left[ 1 - \left( 1 - T_A(\mathbf{s}) \sigma_{\text{inel}}^{\text{NN}} \right)^A \right] d^2s \quad (1.11)$$

111 The correlation between  $N_{\text{coll}}$  and  $N_{\text{part}}$  can be seen in Figure 1.7

112 The charged particle multiplicity  $N_{\text{ch}}$  along with the combination of  $N_{\text{part}}$  and impact parameter  $b$  can  
 113 be used to determine the centrality of a heavy ion event. An example of this is shown in Figure 1.8.

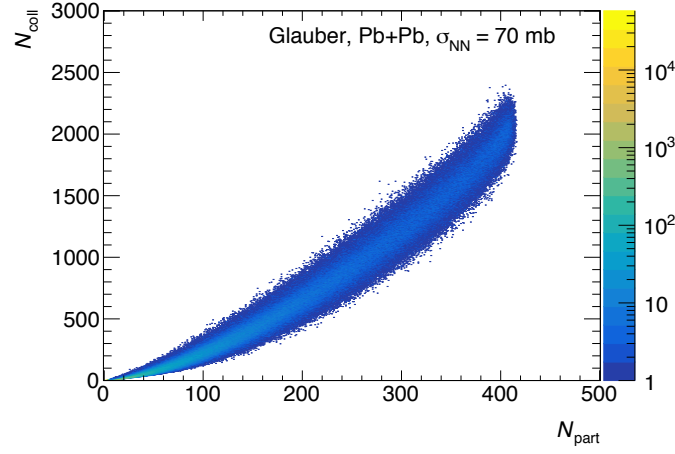


Figure 1.7: The  $N_{\text{coll}} - N_{\text{part}}$  correlation for Pb+Pb collisions at  $\sqrt{s_{\text{NN}}} = 5.02 \text{ TeV}$ . Taken from [25].

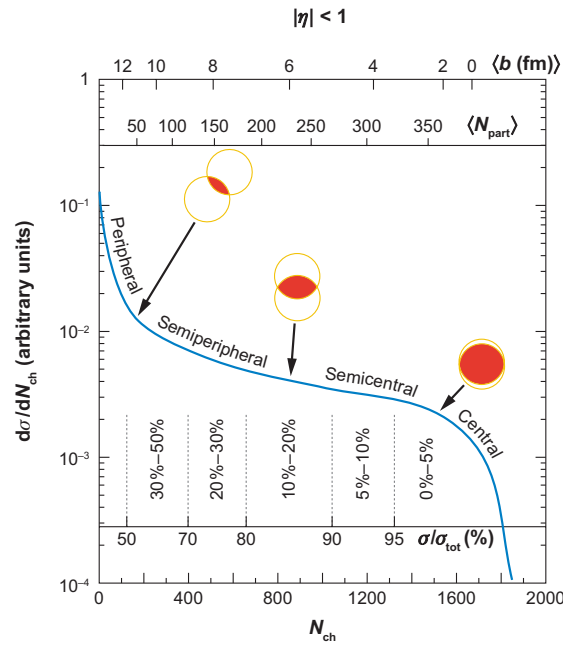


Figure 1.8: The correlation between the observable  $N_{\text{ch}}$  and  $N_{\text{part}}$  to determine the centrality distribution. Taken from [21].

### 114 1.2.2 The Quark Gluon Plasma

115 Quarks and gluons are deconfined at extremely high energy and density conditions and form a state called  
116 the Quark Gluon Plasma [17]. These conditions are met in high energy heavy ion collisions. The Quark  
117 Gluon Plasma has to be described in terms of its constituent quarks and gluons as opposed to the hadrons.  
118 This transition between confinement within hadrons and being free within the QGP occurs at very high  
119 temperatures and pressures. This can be seen in the QCD phase diagram shown in Figure 1.9.

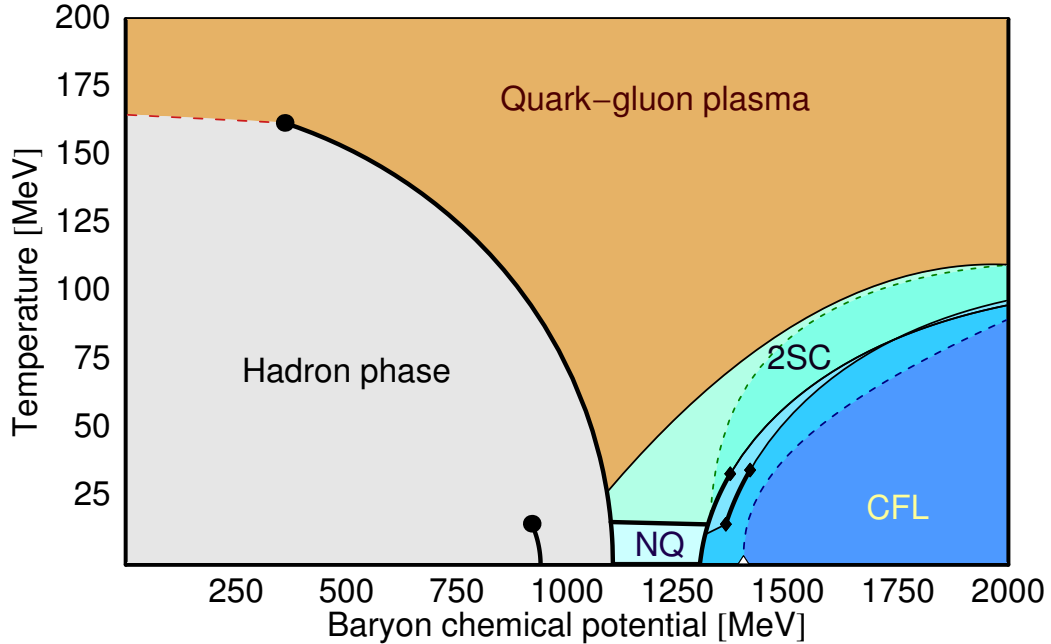


Figure 1.9: The QCD phase diagram of nuclear matter. Figure from Reference [26].

120 This state of matter exists above  $\lambda_{\text{QCD}} = 200 \text{ MeV}$ , the fundamental energy scale in QCD, and is believed  
121 to have filled the early universe a few microseconds after the Big Bang [23, 24] and might be present in the  
122 cores of extremely compact objects like neutron stars.

123 The MIT Bag Model can be used to describe the QGP as a simple ideal gas with a bag constant  $B$  that  
124 parameterizes the vacuum pressure [27, 28].

125 The QGP was initially thought to be a weakly coupled parton gas. This was based on asymptotic  
126 freedom from QCD; the highly energetic collisions such as those at the LHC would imply a weak interaction  
127 between the quarks and gluons that make up the plasma. This would result in rare scatterings between  
128 the constituents of the gas and wash out any spatial anisotropies based on the collision geometry. On the  
129 other hand, if the QGP is assumed to be strongly coupled, the pressure gradients in the medium would  
130 be driven by hydrodynamics and transform spatial anisotropies to momentum anisotropies in the particles

131 produced as shown in Figure 1.10. In this picture, the non-uniform structure of the colliding nuclei would  
 132 cause a momentum anisotropy that would be further enhanced when looking at collisions that are less central  
 133 and do not have perfect overlap between the colliding nuclei [116, 117, 118, 63]. Azimuthal correlation  
 134 measurements [29–34] indicate momentum anisotropy in the collision, implying that the medium is strongly  
 135 coupled.

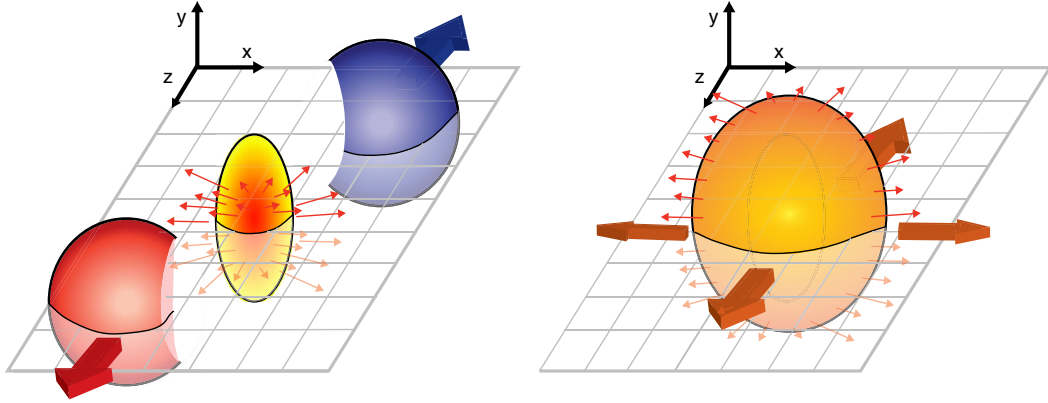


Figure 1.10: Schematic diagrams of the initial overlap region (left) and the final spatial anisotropy generated (right). Taken from [35].

136 A Fourier Transform of the angular distribution of charged hadrons in the collision debris can quantify  
 137 these momentum anisotropies and give the anisotropic flow coefficients  $v_n$ , defined as [115]:

$$\frac{d\bar{N}}{d\phi} = \frac{\bar{N}}{2\pi} \left( 1 + 2 \sum_{n=1}^{\inf} v_n \cos(n(\phi - \bar{\Psi}_n)) \right) \quad (1.12)$$

138 where  $\phi$  is the angle in the transverse plane,  $\bar{\Psi}_n$  are the event plane angles, and  $\bar{N}$  is the average number  
 139 of particles per event. Some of these coefficients are shown in Figure 1.11.

140 Thermal photons from the QGP reveal that it reaches temperatures of 300–600 MeV in central collisions  
 141 at 200 GeV [36] and 2.76 TeV [37], showing very little collision energy dependence. Further, the chemical  
 142 freeze-out temperature was found to be 160 MeV via measurements of ratios of final state hadrons [38–40]  
 143 with the thermal freeze-out being 100–150 MeV [41–44].

### 144 1.3 Jets and Jet Quenching

145 Hard scatterings in the colliding nuclei result in the production of highly energetic partons that evolve, decay,  
 146 and eventually form conical sprays of particles called jets. Jet production is well understood in a  $pp$  collision

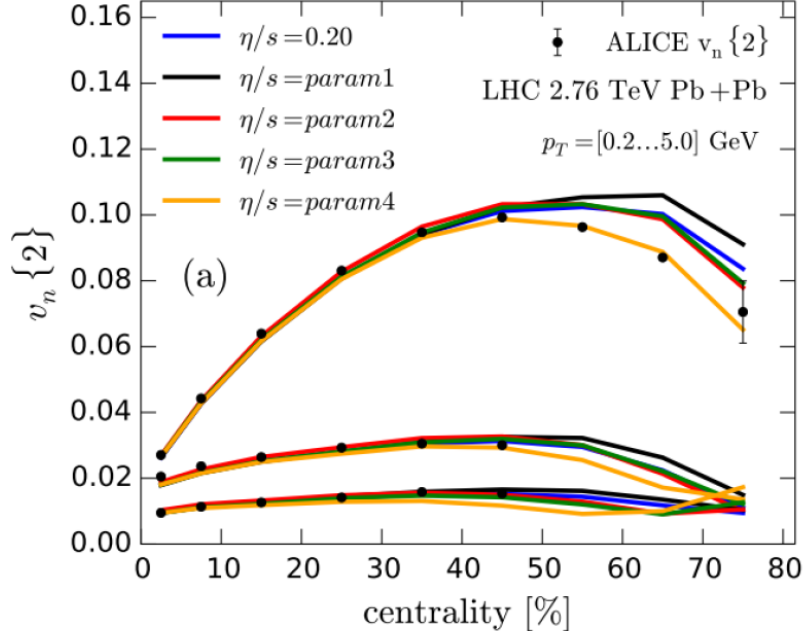


Figure 1.11: Comparison of a hydrodynamic model from [107] to the anisotropy measurements by ALICE [108] for different parameterizations of the  $\eta/s$  and for different  $v_n(n = 2, 3, 4)$  from top to bottom as a function of collision centrality. – see ATLAS measurement from [109].

environment (where there are no QGP effects) in the context of perturbative QCD [161]. In heavy ion collisions, jets must traverse the quark gluon plasma. This can result in the jet losing energy and forward momentum [162, 163], while also picking up momentum transverse to the parton direction. Jets can also deposit energy in the medium, creating a wake [71, 70].

Jet production shown in Figure 1.12 can be written in terms of the parton distribution functions, scattering cross sections, and the fragmentation functions as

$$d\sigma_{pp \rightarrow hX} \approx \sum_{abjd} \int dx_a \int dx_b \int dz_j f_{a/p}(x_a, \mu_f) \times f_{b/p}(x_b, \mu_f) \quad (1.13)$$

$$\times d\sigma_{ab \rightarrow jd}(\mu_f, \mu_F, \mu_R) \quad (1.14)$$

$$\times D_{j \rightarrow h}(Z_j, \mu_f) \quad (1.15)$$

These are discussed in Section 1.3.

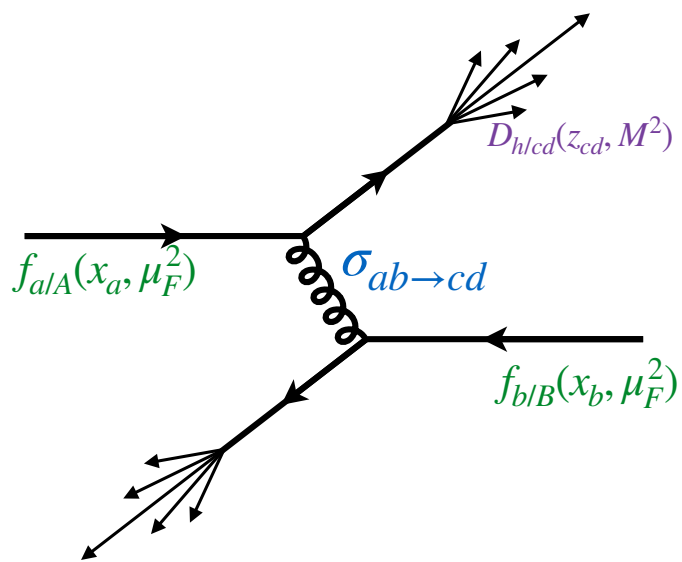


Figure 1.12: Jet production from the process  $pp \rightarrow hX$ , factorizing in terms of the parton distribution functions, scattering cross sections, and jet fragmentation functions. [[arXiv:1511.00790](https://arxiv.org/abs/1511.00790)]

# Bibliography

- 154 [1] M. K. Gaillard, P. D. Grannis and F. J. Sciulli, *The Standard model of particle physics*, Rev. Mod.  
155 Phys. **71** (1999) S96, arXiv: [hep-ph/9812285 \[hep-ph\]](#) (cit. on p. 1).
- 156 [2] J Beringer et al., *Review of Particle Physics, 2012-2013. Review of Particle Properties*, Phys. Rev. D  
157 **86** (2012) 010001 (cit. on pp. 2, 3).
- 158 [3] A. Deur et al., *High precision determination of the  $Q^2$  evolution of the Bjorken Sum*, Phys. Rev. D**90**  
159 (2014) 012009, arXiv: [1405.7854 \[nucl-ex\]](#) (cit. on p. 4).
- 160 [4] J. H. Kim et al., *A Measurement of  $\alpha_s(Q^2)$  from the Gross-Llewellyn Smith sum rule*, Phys. Rev. Lett.  
161 **81** (1998) 3595, arXiv: [hep-ex/9808015 \[hep-ex\]](#) (cit. on p. 4).
- 162 [5] G. Altarelli et al., *Determination of the Bjorken sum and strong coupling from polarized structure  
163 functions*, Nucl. Phys. **B496** (1997) 337, arXiv: [hep-ph/9701289 \[hep-ph\]](#) (cit. on p. 4).
- 164 [6] H. W. Kendall, *Deep inelastic scattering: Experiments on the proton and the observation of scaling*,  
165 Rev. Mod. Phys. **63** (3 1991) 597 (cit. on p. 4).
- 166 [7] A. L. Kataev, G. Parente and A. V. Sidorov, *Improved fits to the  $xF_3$  CCFR data at the next-to-next-to-  
167 leading order and beyond*, Phys. Part. Nucl. **34** (2003) 20, [Erratum: Phys. Part. Nucl.38,no.6,827(2007)],  
168 arXiv: [hep-ph/0106221 \[hep-ph\]](#) (cit. on p. 4).
- 169 [8] S. Alekhin, J. Blumlein and S. Moch, *Parton Distribution Functions and Benchmark Cross Sections at  
170 NNLO*, Phys. Rev. D**86** (2012) 054009, arXiv: [1202.2281 \[hep-ph\]](#) (cit. on p. 4).
- 171 [9] S. Alekhin, J. Blumlein and S.-O. Moch, *ABM news and benchmarks*, PoS **DIS2013** (2013) 039, arXiv:  
172 [1308.5166 \[hep-ph\]](#) (cit. on p. 4).
- 173 [10] J. Blumlein, H. Bottcher and A. Guffanti, *Non-singlet QCD analysis of deep inelastic world data at  
174  $O(\alpha_s^3)$* , Nucl. Phys. **B774** (2007) 182, arXiv: [hep-ph/0607200 \[hep-ph\]](#) (cit. on p. 4).
- 175 [11] H1 Collaboration, *Three- and Four-jet Production at Low  $x$  at HERA*, Eur. Phys. J. C**54** (2008) 389,  
176 arXiv: [0711.2606 \[hep-ex\]](#) (cit. on p. 4).

- 177 [12] ZEUS Collaboration, *Forward-jet production in deep inelastic ep scattering at HERA*, *Eur. Phys. J.*  
 178 **C52** (2007) 515, arXiv: [0707.3093 \[hep-ex\]](#) (cit. on p. 4).
- 179 [13] ZEUS Collaboration, *Multi-jet cross-sections in charged current  $e^\pm p$  scattering at HERA*, *Phys. Rev.*  
 180 **D78** (2008) 032004, arXiv: [0802.3955 \[hep-ex\]](#) (cit. on p. 4).
- 181 [14] ZEUS Collaboration, *Inclusive dijet cross sections in neutral current deep inelastic scattering at HERA*,  
 182 *Eur. Phys. J. C70* (2010) 965, arXiv: [1010.6167 \[hep-ex\]](#) (cit. on p. 4).
- 183 [15] ZEUS Collaboration, *Inclusive-jet cross sections in NC DIS at HERA and a comparison of the  $kT$ ,*  
 184 *anti- $kT$  and SIScone jet algorithms*, *Phys. Lett. B691* (2010) 127, arXiv: [1003.2923 \[hep-ex\]](#) (cit. on  
 185 p. 4).
- 186 [16] H1 Collaboration, *Jet Production in ep Collisions at High  $Q^2$  and Determination of  $\alpha_s$* , *Eur. Phys. J.*  
 187 **C65** (2010) 363, arXiv: [0904.3870 \[hep-ex\]](#) (cit. on p. 4).
- 188 [17] E. V. Shuryak, *Quantum chromodynamics and the theory of superdense matter*, *Physics Reports*  
 189 **61** (1980) 71 , ISSN: 0370-1573, URL: <http://www.sciencedirect.com/science/article/pii/0370157380901052> (cit. on pp. 4, 9).
- 190 [18] R. Glauber, *Lectures in theoretical physics*, ed. WE Brittin and LG Dunham, Interscience, New York **1**  
 191 (1959) 315 (cit. on p. 5).
- 192 [19] R. Glauber et al., *Lectures in theoretical physics*, 1959 (cit. on p. 5).
- 193 [20] H. D. Vries, C. D. Jager and C. D. Vries, *Nuclear charge-density-distribution parameters from elastic*  
 194 *electron scattering*, *Atomic Data and Nuclear Data Tables* **36** (1987) 495 , ISSN: 0092-640X, URL:  
 195 <http://www.sciencedirect.com/science/article/pii/0092640X87900131> (cit. on pp. 5, 6).
- 196 [21] M. L. Miller, K. Reygers, S. J. Sanders and P. Steinberg, *Glauber Modeling in High-Energy Nuclear*  
 197 *Collisions*, *Annual Review of Nuclear and Particle Science* **57** (2007) 205, eprint: <https://doi.org/10.1146/annurev.nucl.57.090506.123020>, URL: <https://doi.org/10.1146/annurev.nucl.57.090506.123020> (cit. on pp. 5, 6, 8).
- 198 [22] B. Alver, M. Baker, C. Loizides and P. Steinberg, *The PHOBOS Glauber Monte Carlo*, (2008), arXiv:  
 199 [0805.4411 \[nucl-ex\]](#) (cit. on p. 5).
- 200 [23] D. Kharzeev and M. Nardi, *Hadron production in nuclear collisions at RHIC and high density QCD*,  
 201 *Phys. Lett. B507* (2001) 121, arXiv: [nucl-th/0012025 \[nucl-th\]](#) (cit. on p. 7).
- 202 [24] A. Bialas, M. Bleszynski and W. Czyz, *Multiplicity Distributions in Nucleus-Nucleus Collisions at*  
 203 *High-Energies*, *Nucl. Phys. B111* (1976) 461 (cit. on p. 7).

- 207 [25] ATLAS Collaboration, *Centrality determination in  $\sqrt{s_{NN}} = 5.02$  TeV Pb+Pb collision data in 2015*,  
 208 tech. rep. ATL-COM-PHYS-2016-1287, CERN, 2016, URL: <https://cds.cern.ch/record/2212936>  
 209 (cit. on p. 8).
- 210 [26] S. B. Ruster, V. Werth, M. Buballa, I. A. Shovkovy and D. H. Rischke, *Phase diagram of neutral*  
 211 *quark matter: Self-consistent treatment of quark masses*, Phys. Rev. D **72** (3 2005) 034004, URL:  
 212 <https://link.aps.org/doi/10.1103/PhysRevD.72.034004> (cit. on p. 9).
- 213 [27] B. Müller, ‘Physics of the Quark-Gluon Plasma’, *Particle Production in Highly Excited Matter*, ed.  
 214 by H. H. Gutbrod and J. Rafelski, Springer US, 1993 11, ISBN: 978-1-4615-2940-8, URL: [https://doi.org/10.1007/978-1-4615-2940-8\\_2](https://doi.org/10.1007/978-1-4615-2940-8_2) (cit. on p. 9).
- 216 [28] K. Yagi, T. Hatsuda and Y. Miake, *Quark-gluon plasma: From big bang to little bang*, Camb. Monogr.  
 217 Part. Phys. Nucl. Phys. Cosmol. **23** (2005) 1 (cit. on p. 9).
- 218 [29] ATLAS Collaboration, *Measurement of flow harmonics with multi-particle cumulants in Pb+Pb collisions*  
 219 *at  $\sqrt{s_{NN}} = 2.76$  TeV with the ATLAS detector*, The European Physical Journal C **74** (2014) 3157,  
 220 ISSN: 1434-6052, URL: <https://doi.org/10.1140/epjc/s10052-014-3157-z> (cit. on p. 10).
- 221 [30] STAR Collaboration, *Identified Particle Elliptic Flow in Au + Au Collisions at  $\sqrt{s_{NN}} = 130$  GeV*, Phys.  
 222 Rev. Lett. **87** (18 2001) 182301, URL: <https://link.aps.org/doi/10.1103/PhysRevLett.87.182301>  
 223 (cit. on p. 10).
- 224 [31] PHENIX Collaboration, *Elliptic Flow of Identified Hadrons in Au + Au Collisions at  $\sqrt{s_{NN}} = 200$  GeV*,  
 225 Phys. Rev. Lett. **91** (18 2003) 182301, URL: <https://link.aps.org/doi/10.1103/PhysRevLett.91.182301> (cit. on p. 10).
- 227 [32] PHOBOS Collaboration, *System Size, Energy, Pseudorapidity, and Centrality Dependence of Elliptic  
 228 Flow*, Phys. Rev. Lett. **98** (24 2007) 242302, URL: <https://link.aps.org/doi/10.1103/PhysRevLett.98.242302> (cit. on p. 10).
- 230 [33] CMS Collaboration, *Measurement of higher-order harmonic azimuthal anisotropy in PbPb collisions at*  
 231  *$\sqrt{s_{NN}} = 2.76$  TeV*, Phys. Rev. C **89** (4 2014) 044906, URL: <https://link.aps.org/doi/10.1103/PhysRevC.89.044906> (cit. on p. 10).
- 233 [34] ALICE Collaboration, *Anisotropic Flow of Charged Particles in Pb-Pb Collisions at  $\sqrt{s_{NN}} = 5.02$  TeV*,  
 234 Phys. Rev. Lett. **116** (13 2016) 132302, URL: <https://link.aps.org/doi/10.1103/PhysRevLett.116.132302> (cit. on p. 10).

- 236 [35] M. Connors, C. Nattrass, R. Reed and S. Salur, *Jet measurements in heavy ion physics*, Rev. Mod. Phys.  
 237 **90** (2 2018) 025005, URL: <https://link.aps.org/doi/10.1103/RevModPhys.90.025005> (cit. on  
 238 p. 10).
- 239 [36] PHENIX Collaboration, *Enhanced Production of Direct Photons in Au + Au Collisions at  $\sqrt{s_{NN}} =$*   
 240 *200 GeV and Implications for the Initial Temperature*, Phys. Rev. Lett. **104** (13 2010) 132301, URL:  
 241 <https://link.aps.org/doi/10.1103/PhysRevLett.104.132301> (cit. on p. 10).
- 242 [37] ALICE Collaboration, *Direct photon production in Pb-Pb collisions at  $s_{NN}=2.76 \text{ TeV}$* , Physics Letters  
 243 **B** **754** (2016) 235 , ISSN: 0370-2693, URL: <http://www.sciencedirect.com/science/article/pii/S0370269316000320> (cit. on p. 10).
- 245 [38] Z. Fodor and S. Katz, *Critical point of QCD at finite T and  $\mu$ , lattice results for physical quark*  
 246 *masses*, Journal of High Energy Physics **2004** (2004) 050, URL: <https://doi.org/10.1088%2F1126-6708%2F2004%2F04%2F050> (cit. on p. 10).
- 248 [39] STAR Collaboration, *Experimental and theoretical challenges in the search for the quark-gluon plasma: The STAR Collaboration's critical assessment of the evidence from RHIC collisions*, Nuclear Physics  
 249 **A** **757** (2005) 102 , First Three Years of Operation of RHIC, ISSN: 0375-9474, URL: <http://www.sciencedirect.com/science/article/pii/S0375947405005294> (cit. on p. 10).
- 252 [40] ALICE Collaboration, *Production of light nuclei and anti-nuclei in pp and Pb-Pb collisions at energies*  
 253 *available at the CERN Large Hadron Collider*, Phys. Rev. C **93** (2 2016) 024917, URL: <https://link.aps.org/doi/10.1103/PhysRevC.93.024917> (cit. on p. 10).
- 255 [41] PHENIX Collaboration, *Single identified hadron spectra from  $\sqrt{s_{NN}} = 130 \text{ GeV}$  Au + Au collisions*,  
 256 Phys. Rev. C **69** (2 2004) 024904, URL: <https://link.aps.org/doi/10.1103/PhysRevC.69.024904>  
 257 (cit. on p. 10).
- 258 [42] BRAHMS Collaboration, *Centrality dependent particle production at  $y = 0$  and  $y \geq 1$  in Au+Au collisions*  
 259 *at  $\sqrt{s_{NN}} = 200 \text{ GeV}$* , Phys. Rev. C **72** (1 2005) 014908, URL: <https://link.aps.org/doi/10.1103/PhysRevC.72.014908> (cit. on p. 10).
- 261 [43] PHOBOS Collaboration, *Identified hadron transverse momentum spectra in Au+Au collisions at*  
 262  *$\sqrt{s_{NN}} = 62.4 \text{ GeV}$* , Phys. Rev. C **75** (2 2007) 024910, URL: <https://link.aps.org/doi/10.1103/PhysRevC.75.024910> (cit. on p. 10).
- 264 [44] ALICE Collaboration, *Centrality dependence of  $\pi$ ,  $K$ , and  $p$  production in Pb-Pb collisions at  $\sqrt{s_{NN}} =$*   
 265 *2.76 TeV*, Phys. Rev. C **88** (4 2013) 044910, URL: <https://link.aps.org/doi/10.1103/PhysRevC.88.044910> (cit. on p. 10).